JGR Planets

RESEARCH ARTICLE
10.1029/2024JE008739

Statistical Methods to Distinguish Shallow Moonquakes From Impacts

Alice R. Turner[1,2], **Sean P. S. Gulick**[1,3,4], **Daniel T. Trugman**[5], **Francesco Civilini**[6], **and Keisuke Onodera**[7]

[1]University of Texas at Austin Institute for Geophysics, Austin, TX, USA, [2]Department of Earth Sciences, University of Cambridge, Cambridge, UK, [3]University of Texas at Austin Department of Earth and Planetary Sciences, Austin, TX, USA, [4]University of Texas at Austin Center for Planetary Systems Habitability, Austin, TX, USA, [5]Nevada Seismological Laboratory, University of Nevada, Reno, NV, USA, [6]NASA Goddard Space Flight Center, Greenbelt, MD, USA, [7]Institute for Planetary Materials, Okayama University, Misasa, Japan

Key Points:

- We present quantitative methods to differentiate impacts from shallow moonquakes, aiding lunar seismic data analysis now and in the future
- We use a Kullback–Leibler metric to compare pairs of spectrograms and find high similarity between pairs of shallow moonquakes
- We analyze the variability of shallow moonquake spectra and suggest that it may arise from a range of source depths

Supporting Information:

Supporting Information may be found in the online version of this article.

Correspondence to:

A. R. Turner,
art77@cam.ac.uk

Citation:

Turner, A. R., Gulick, S. P. S., Trugman, D. T., Civilini, F., & Onodera, K. (2025). Statistical methods to distinguish shallow moonquakes from impacts. *Journal of Geophysical Research: Planets*, *130*, e2024JE008739. https://doi.org/10.1029/2024JE008739

Received 18 SEP 2024
Accepted 4 JUL 2025

Abstract One of the biggest challenges in lunar seismology is accurately classifying seismic signals to evaluate impact and seismicity rates. While past studies have used qualitative differences for classification, we introduce quantitative methods to distinguish the most energetic signals: shallow moonquakes and natural impacts. Our approach utilizes previously under-analyzed data from the short-period Apollo seismic instruments, which operated on the Moon between 1969 and 1977. First, we convert short-period spectrograms to smoothed probability density functions. Next, we use the Kullback–Leibler divergence as a metric to measure the differences in the spectrograms between the two types of event. Using this comparison metric, we find that shallow moonquakes are more similar to other shallow moonquakes than to impacts. By analyzing individual waveforms, we identify features that significantly differ between shallow moonquakes and impacts, such as spectral entropy and autocorrelation. These features, which have characteristic ranges of values for each class of event, can be used to categorize the signal without comparison to another event. We apply these statistical metrics to a set of previously unclassified high-frequency events and shallow moonquakes that were identified last year. We find that high-frequency events and newly identified shallow moonquakes have a variety of features. Many of the shallow moonquakes that were identified last year are consistent with those identified over 50 years ago and may have a range of source depths. Along with supporting reanalysis of the Apollo seismic signals, these statistical metrics may be useful for future analysis of lunar seismic data.

Plain Language Summary The Apollo seismic instruments recorded the ground shaking produced by meteoroids bombarding the Moon's surface and naturally occurring quakes. Deciphering the cause of the recorded shaking, whether meteors or quakes, has always been challenging due to poor data quality, but it is essential to understand the impact rate and seismicity on the Moon. In the past, researchers distinguished the events visually, which is time-consuming and prone to bias. In this study, we use measurable differences between the two types of signals to make telling them apart easier and quicker than visual inspection alone. We use these new measurements to identify one possible new shallow moonquake and confirm that a set of events visually identified last year are consistent with those identified over 50 years ago. The variability in the signal properties of shallow moonquakes may also indicate a range of source depths.

1. Introduction

Astronauts deployed seismometers on the near side of the Moon during Apollo missions 11, 12, 14, 15, and 16 as part of the passive seismic experiment (Latham et al., 1969). The station deployed at the Apollo 11 site only operated for 21 days (Latham, Ewing, Press, et al., 1970), but the remaining four stations formed the lunar seismic network. These instruments monitored the Moon until the telemetry was turned off in 1977, providing nearly eight years of continuous lunar seismic data. The Apollo seismic network provided the first observations of seismicity on another planetary body and still offers valuable insights into the interior and dynamics of the Moon.

Each station in the lunar seismic network consisted of a 3-component mid-period instrument and a single vertical-component short-period instrument (Nunn et al., 2020). The short-period sensor has a displacement response peaked at approximately 8 Hz. The mid-period sensor operated in two response modes: peaked and flat. The peaked mode of the mid-period sensor has a peak at about 0.45 Hz while the flat mode has flat response between 0.1 and 1 Hz.

During the operation of these instruments, ∼13,000 seismic events were identified (Nakamura et al., 1981). The events share similar features; most noticeably, all the events have an especially long coda created by the highly fractured outer shell of the Moon, which allows seismic energy to reverberate (Blanchette-Guertin et al., 2012; Gillet et al., 2017; Onodera et al., 2022). Despite the highly scattered nature of the lunar waveforms, the signals were grouped into four main categories based on their amplitude and frequency content: (a) small, local thermal moonquakes triggered by lunar day-night cycle temperature changes (e.g., Civilini et al., 2023; Duennebier & Sutton, 1974b); (b) repeating tidal deep moonquakes originating from 700 to 1,200 km depth (e.g., Bulow et al., 2005; Nakamura, 2003; Turner et al., 2022); (c) man-made and natural impacts (e.g., Duennebier & Sutton, 1974a; Gudkova et al., 2011, 2015; Latham, Ewing, Dorman, et al., 1970); and (d) shallow moonquakes (e.g., Nakamura, 1977; Onodera, 2024; Watters et al., 2019).

Shallow moonquakes are the least common of these four types of lunar seismic events, only documented 28 times in the original catalog (Nakamura, 1977; Nakamura et al., 1981). It has been theorised that these shallow moonquakes could be related to young thrust faults on the Moon, which would imply that shallow moonquakes are of tectonic origin (Watters et al., 2019). On Earth, tectonic earthquakes have a characteristic logarithmic relationship between any measure of the earthquake magnitude and total number of earthquakes (known as the "Gutenberg–Richter distribution"). The slope of the relationship (b-value) is typically around 1 (Shearer, 2019; Stein & Wysession, 2009), meaning that for a given frequency of magnitude 4.0 or larger events, there will be 10 times as many magnitude 3.0 or larger quakes and 100 times as many magnitude 2.0 or larger quakes. For the 28 shallow moonquakes, the slope of the relationship between the number of moonquakes and the body wave magnitude is only 0.5 (Nakamura, 1977, 1980) therefore the catalog of shallow moonquakes lacks small-magnitude events relative to tectonic events on Earth. If shallow moonquakes are tectonic in origin, where are all the small-magnitude shallow moonquakes? One possibility is that these are present but have not yet been identified in the Apollo seismic data set. Identifying and categorizing new events remains challenging due to the poor data quality of the Apollo seismic data.

The classification of the lunar seismic events was conventionally performed visually based on the waveform features and spectral content, both during the creation of the original mid-period event catalog (Nakamura et al., 1981) and during more recent reanalysis (Onodera, 2024). Deep moonquakes have a lower frequency content, with the energy concentrated below 1 Hz, and as such, are not typically observed in the short-period data (Bulow et al., 2005, 2007; Nakamura, 2003; Nunn et al., 2020), while most thermal moonquakes typically do not appear on the mid-period instrument (Nunn et al., 2020). Natural impacts and shallow moonquakes are observed on both instruments with similar frequency characteristics, making them harder to distinguish. Numerous challenges related to the quality of the lunar seismic data, including varying sampling rates, limited frequency bands, high amplitude spikes, and limited digitization make distinguishing and cataloging lunar seismic events by eye a challenging and time-consuming process, increasing the probability that events may have been missed or incorrectly categorized.

In this study, we use new methods to analyze the time and frequency content of shallow moonquakes and impacts. We aim to understand the quantitative differences between the two classes of signals as well as variations within the two populations. Identifying quantitative metrics that characterize the signals may also help reduce the burden of analyzing and classifying tens of thousands of seismic signals by eye. This work is important as the planetary community will be launching several new seismic missions over the next decade that are focused on the Moon. These future seismic missions include: NASA's Farside Seismic Suite to the Schrödinger impact basin in 2026 (Panning et al., 2022); the Lunar Environment Monitoring Station (LEMS) to be deployed during Artemis III in 2026 (Schmerr et al., 2024); and China's Chang'e 7 and 8 missions, which are scheduled in 2026 and 2028 respectively (Li et al., 2019). The development of new methods and workflows to distinguish and catalog seismic events represents key preparation for the upcoming lunar seismic data collection.

1.1. Theoretical Differences Between Shallow Moonquakes and Natural Impacts

We begin by discussing the differences between impacts and shallow moonquakes that would be expected from seismic source theory. Shallow moonquakes are thought generated by shear displacement on a fault plane (Lammlein et al., 1974; Nakamura, 1977) and can be described mathematically as a double couple source, like tectonic earthquakes (Aki & Richards, 2002). In contrast to a moonquake, which is generated by slip on a fault, impactors strike the ground directly to generate seismic signals. This implies that the seismic signal of an impact is

better described mathematically by a single force acting downwards on the surface (Edwards et al., 2008; Gudkova et al., 2011).

The single couple versus double couple mathematical descriptions predict different focal mechanisms and seismic source characteristics. While the analysis of seismic focal mechanisms can be informative about the physics of the source generating the signal (e.g., Thurin et al., 2022), there has been little success in seismically determining lunar focal mechanisms (Araki, 2001; Koyama & Nakamura, 1980; Weber et al., 2009). Methods to determine focal mechanisms require clear observations of the first-motion polarities at many stations with a good azimuthal distribution around the epicenter—the sparse seismic network and highly scattered waveforms limit both of these. However, even without determining focal mechanisms, the time series and spectral features of shallow moonquakes and impacts are expected to be different. In the time domain, impacts are expected to have positive first arrivals (Daubar et al., 2018) and are likely to produce stronger P-waves and relatively weaker S-waves when compared to tectonic events (Daubar et al., 2018; Nakamura, 1977; Nunn et al., 2024). The two sources also result in spectra with different frequency contents and shapes. For events occurring at the same location, shallow moonquakes should be enriched in higher frequencies above 1–5 Hz relative to impacts (Daubar et al., 2018; Gudkova et al., 2011, 2015; Knapmeyer-Endrun & Hammer, 2015).

In addition to the different seismic sources, the seismic energy may take different paths through the Moon to reach the station. Impacts happen at the surface, and the seismic energy travels longer distances in the shallow scattering layer, increasing the length of the coda (Blanchette-Guertin et al., 2012; Daubar et al., 2018; Gudkova et al., 2011). The depth of shallow moonquakes, and the path that the seismic energy may take is more poorly constrained, with depth estimate <200 km below the crust (Gillet et al., 2017; Nakamura et al., 1979; Watters et al., 2010). The possible deeper source depth of shallow moonquakes means that the seismic energy travels a shorter distance in the scattering layer. As such, an impact would be expected to experience more scattering and have a longer coda than shallow moonquakes at the same epicentral distance (Blanchette-Guertin et al., 2012; Gillet et al., 2017; Onodera, 2024)

1.2. Observable Differences Between Shallow Moonquakes and Natural Impacts

Many differences between shallow moonquakes and impacts predicted from seismic source theory can be seen in the Apollo seismic data. Figure 1 shows the average and median mid-period spectral amplitude for shallow moonquakes and impacts. The spectra are averaged across all traces recorded on the 3 mid-period components at 4 seismic stations (all the traces that are averaged are plotted in Figure S1 in Supporting Information S1). The frequency response of the mid-period instrument in the flat response mode has a sensitivity between 0.1 and 1 Hz (Nunn et al., 2020), which creates the plateau below 0.1 Hz and the drop off above 1 Hz. On average, shallow moonquakes have a higher spectral amplitude between 0.1 and 1 Hz.

The expected differences between shallow moonquakes and impacts can also be seen in individual signals recorded on the short-period instrument. Figure 2 shows an example of a shallow moonquake and impact signal at different epicentral distances. Both the signal of the shallow moonquake and the impact are higher than the background, and the unprocessed waveforms plotted in panels A and E look similar to the processed velocity waveforms in B and F (see Section 2.1 for a description of the processing steps). The shallow moonquake signal in panel B has two packets of arriving energy; a smaller scattered P wave arrival at ∼200 s and a larger amplitude scattered S arrival at ∼500 s. The impact in panel D has only a single emergent arrival at ∼100 s. The differences between shallow moonquakes and impacts are also visible in the frequency domain. Figure 2 panels C and G show the spectrograms—the frequency content of the signal is calculated for each 3-s window. The spectral power in each time period is represented by a color. The high-quality shallow moonquake spectrum in Figure 2c have persistent high amplitudes from 500 to 1,000 s in the frequency range from 3 to 9 Hz, making the spectrogram appear almost square, as the energy decay of the shallow moonquake is less frequency dependent. The spectrogram of the high-quality impact looks very different. There is a lack of signal above ∼5 Hz, and the amplitude decays quickly. For high-quality signals, the differences between shallow moonquakes and impacts are clear.

However, only ∼45% of the traces from the 28 shallow moonquakes in the original catalog have a similarly high signal-to-noise ratio (Onodera, 2024). Figure 3 shows examples of a distant lower amplitude shallow moonquake and impact. Throughout the shallow moonquake event in panel A, there are spikes, which are related to the thermal response of the Apollo seismic instrument. The amplitude of both of these events is just above the amplitude of the noise; the shallow moonquake (A) signal is ∼5 times larger than the noise, while the impact (E) is

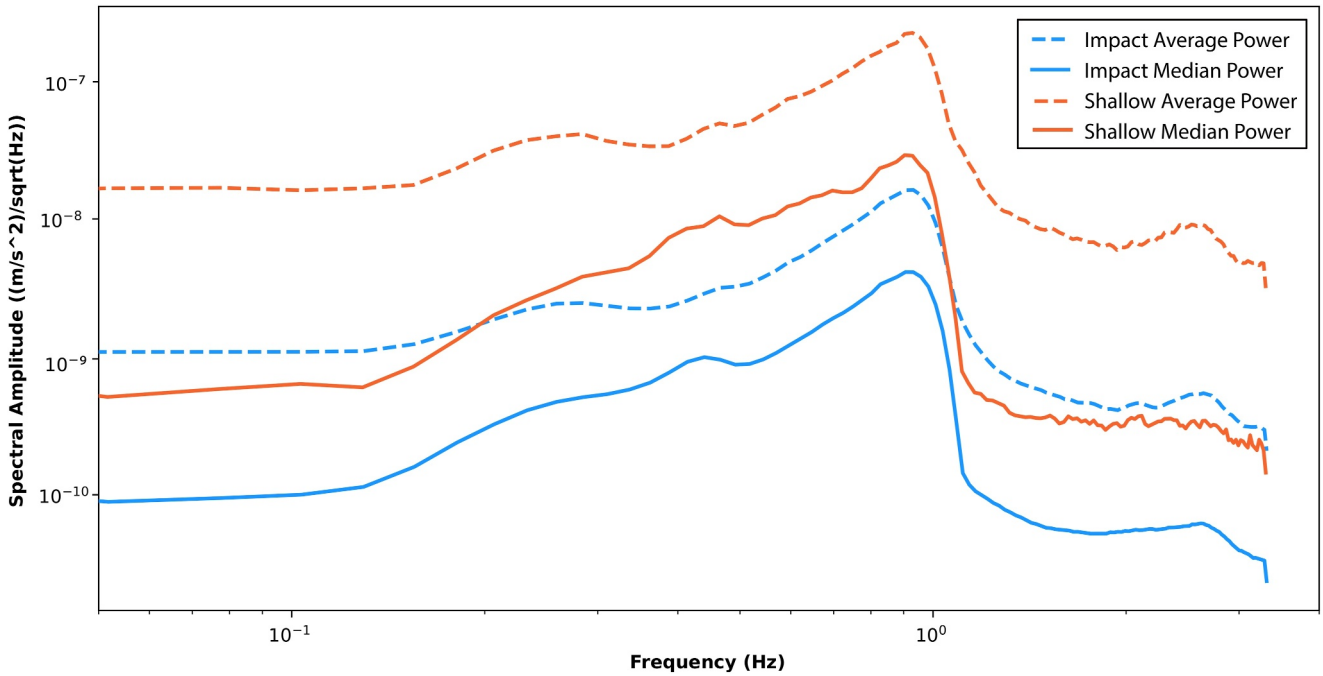

Figure 1. Average and median spectral amplitude of shallow moonquakes and impacts. The orange spectra are the average of ~672 traces—from 64 shallow moonquake events recorded on all 3 components of the mid-period instrument of all 4 seismic stations. The blue spectra is the average of 1,797 impact events. The individual spectra of these events is plotted in Figure S1 in Supporting Information S1.

only ~2.5 times larger than the background noise. The amplitude of both signals is close to the digitization level of the instrument; the maximum variation of the shallow moonquake is 5 counts, and the variation of the impact is just a few counts. As such, it can be harder to distinguish a shallow moonquake from an impact in the time domain, as the direct P and S arrivals are harder to distinguish from the noise and may be interpreted as a single emergent arrival more similar to the impact signal (Figure 3d). In the examples plotted in Figure 3, the spectral features alone can still be used to distinguish the events. As seen in Figure 2, the shallow moonquake has higher frequencies and a slower decay than the impact. But when distinguishing the events based on the frequency content alone, care must be taken; the differences in spectral content also depend on the distance from the recording station, and the signal of proximal impacts can also contain a significant amount of high-frequency energy above 5 Hz (Daubar et al., 2018; Duennebier & Sutton, 1974a; Knapmeyer-Endrun & Hammer, 2015).

Discriminating impacts from moonquakes visually works well for large-magnitude, high-quality events where direct phases can be easily seen. However, it is more difficult to discriminate low quality events at unknown distances. In these cases, it can be a challenge to identify the direct P and S waves, and close impacts may also contain significant high-frequency energy. Parallels can be drawn with the task of discriminating underground nuclear explosions from earthquakes. Many methods exist to discriminate large-magnitude, well-recorded events at teleseismic distances. Still, challenges remain to discriminate small seismic events recorded at small epicentral distances (Douglas, 2013; Koper et al., 2024; Maceira et al., 2017).

In this work, we use both the frequency spectrum and the time-domain waveform to attempt to distinguish shallow moonquakes from impacts. In Section 2, we provide a new metric based on the Kullback–Leibler (K-L) divergence (Kullback & Leibler, 1951) to compare the full spectra of pairs of events. The motivation for choosing the K-L divergence is that it takes into account the full time-frequency characteristics of the event and the shape of the frequency content, which may be more similar to a human analyst. In Section 3, we calculate a range of metrics for individual waveforms including time-series complexity, autocorrelation and spectral entropy using the Python package tsfresh (Christ et al., 2018; Koper et al., 2024). We then determine which metrics significantly differ between shallow moonquakes and impacts. In Section 4 we test the robustness of these statistical metrics, and in Sections 5 and 6 and apply these metrics on previously uncategorized high-frequency signals and new shallow moonquakes identified by Onodera (2024). Finally in Sections 7 and 8, we discuss the implications for lunar

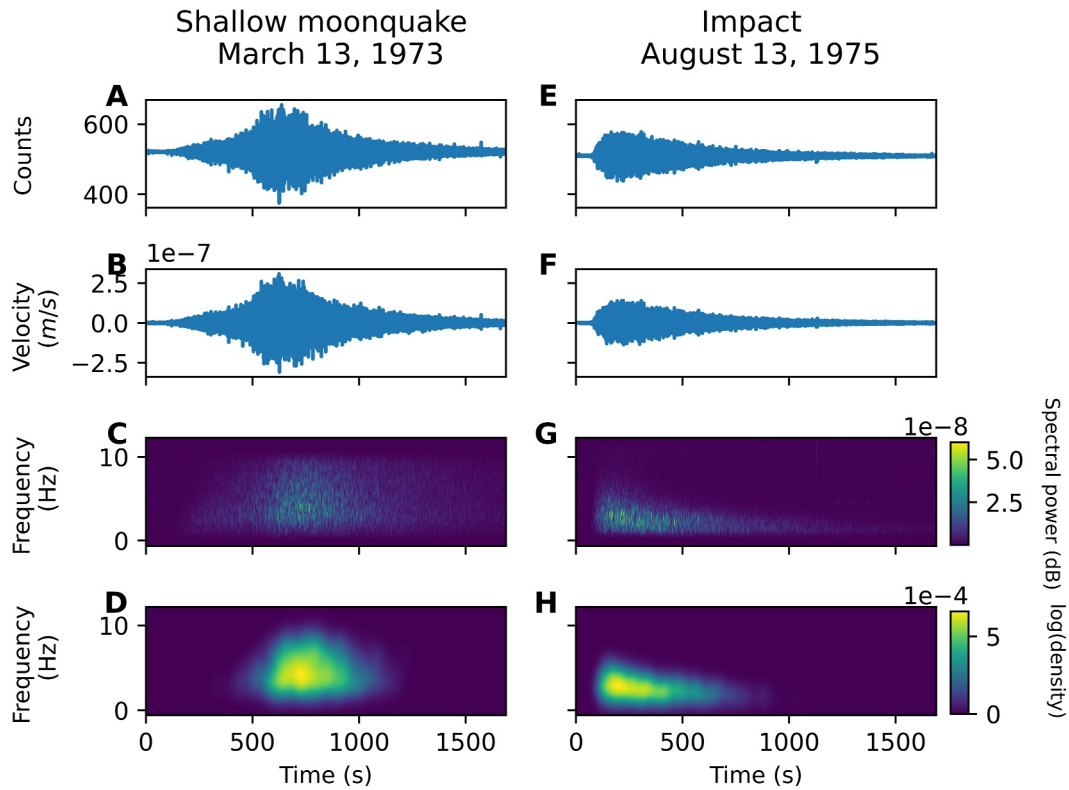

Figure 2. Examples of high-quality signals of moonquakes and impacts at different distances, showing the distinct time and frequency domain characteristics of the two classes of events. (a) An unprocessed shallow moonquake waveform recorded at station S15 on 13 March 1973. (b) The processed velocity waveform. The signal has been despiked, the instrument response removed, and bandpass filtered between 1 and 13 Hz. (c) Spectrogram of the shallow moonquake. (d) Smoothed Kernel density approximation of the shallow moonquake spectrogram. Panels (e–h) are the same as (a–d) for an impact recorded at station S15 on 13 August 1975.

tectonics and shallow moonquake source mechanisms and the application to future lunar data. In combination, the two new methods presented in this work can be used to quantitatively classify lunar seismic signals.

2. Frequency Domain Comparison of Lunar Seismic Signals

2.1. Converting a Moonquake to a Probability Distribution

We downloaded the short-period vertical component Apollo seismic data from stations S14, S15, and S16 from EarthScope (formerly IRIS, Nunn et al., 2022). The waveforms for these events, colored by event type with impacts in blue and shallow moonquakes in orange are plotted in Figures S3, S4 and S5 in Supporting Information S1 for stations S14, S15 and S16 respectively. We focus on the short-period data recorded at stations S14, S15 and S16. The reasons for focusing on the short-period data are twofold; first, the short-period data, until recently has been underutilized for analysis (Onodera, 2024), and provides the best opportunity to possibly identify new shallow moonquakes, and second, the signals of shallow moonquakes and impacts differ the most at the high frequencies (See Figures 1 and 2). In this analysis, we do not consider station S12 as the SPZ component (short-period vertical motion) failed to respond to calibration pulses and operated at a much reduced gain, obtaining little or no valid data (Nunn et al., 2020; Vostreys, 1980).

To identify the seismic signals as shallow moonquakes or impacts, we use the Nakamura et al. (1981) catalog. Each shallow moonquake (denoted with the letter H) and impact (denoted with the letter C) is windowed for 2,000 s after the start time reported in the catalog. Any gaps are filled in with linear interpolation, and the signals are despiked using a median filter with a kernel length of 100 samples (Bulow et al., 2005). The raw data are converted to velocity waveforms with a pre-filter of 1–13 Hz by deconvolving the design response of each of the Apollo seismic instruments available from EarthScope. However, the true response of the instrument varied

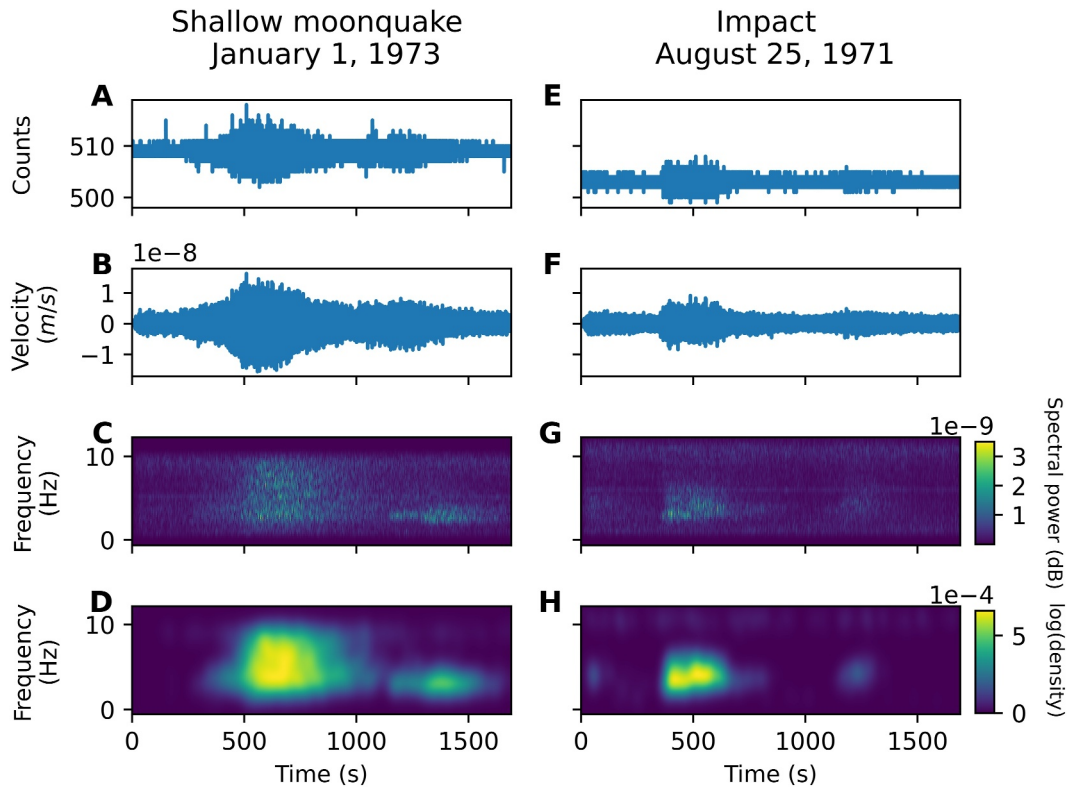

Figure 3. Examples of low-quality signals of moonquakes and impacts at different distances; both the time and frequency domain signals look similar. (a) The unprocessed waveform of a shallow moonquake recorded at station S15 on 27 May 1975. The amplitude of the signal is only a few bits. (b) The processed velocity waveform. The signal has been despiked, the instrument response has been removed and bandpass filtered between 1 and 13 Hz. (c) Spectrogram of the shallow moonquake. (d) Smoothed Kernel density approximation of the shallow moonquake spectrogram. Panels (e–h) are the same as (a–d) for an impact recorded at station S15 on 13 September 1977.

throughout the experiment, such that the true instrument response and the design response were slightly different (Nunn et al., 2020). Using the nominal parameters of the design response, one will introduce minor inaccuracies into the seismic waveform or spectra. These inaccuracies can be seen in Figure S2 in Supporting Information S1 as bands of high amplitude in the spectrograms, especially at station S16. Due to the inaccuracies seen in Figure S2 in Supporting Information S1, we consider events recorded at each seismic station one at a time—we have three separate data sets, at S14, S15 and S16. It is also possible that some of the differences between the spectra at the different stations could be associated with the local geology beneath the station. For example, the band of high amplitude at station S16 in Figure S2 in Supporting Information S1 could be caused a resonance below the surface, but we cannot tell with the limited data. This is all the more reason to consider each station in isolation.

Finally, we calculate the maximum ratio of the short-term average to the long-term average (STA/LTA) for each event as a measure of the signal-to-noise ratio of each of the events. Events with low maximum STA/LTA are likely to be noisy, poor-quality events with reduced confidence in the original classification. Events with a very large maximum STA/LTA likely include significant spikes and glitches that were not effectively removed from the time series in the preprocessing steps—for example, high amplitude spikes that are more than a couple of samples long. Choosing the STA/LTA thresholds is slightly arbitrary—we chose a threshold between 1 and 5 to create a data set of events that we are confident have the correct classification in the original catalog.

For each event, we then calculate the frequency spectrum in each period using the built-in ObsPy function (Beyreuther et al., 2010), as described above and plotted in Figures 2 and 3. The final step is to convert the spectrogram into a 2D probability density function. To do this, we apply a binary mask to the amplitude of the frequency spectra, and we keep only points larger than 20% of the maximum amplitude of each event, creating a density plot. The thresholding procedure serves two purposes: first, by thresholding the spectra at 20% of the

maximum amplitude, we keep all the high amplitude signal and remove some of the noise in the spectra, and second, converting the spectrogram to a collection of points allows us to estimate a probability density function using a kernel density estimate. The kernel density estimate is a non-parametric method for estimating the probability density function based on the density of samples at each location. The denser the points in the binary masked spectrogram, the higher the probability density at that location. The kernel density estimate is implemented using the Kernel Density function of the sklearn module (Pedregosa et al., 2011) with a bandwidth of 1 and the default Gaussian kernel. The kernel density estimate is then smoothed using a Gaussian filter with a sigma of 5. Examples of the smoothed kernel density estimate are shown in Figures 2 and 3.

2.2. K-L Divergence

Having created kernel density estimates of the event spectrograms, we can now compare pairs of events using the Kullback-Leibler (K-L) divergence. The K-L divergence is a measure of the dissimilarity between two probability distributions and is commonly used as a component of the loss function to measure the difference between the generated distribution and the real data distributions in machine learning (Borji, 2022; Salimans et al., 2016). Mathematically, the K-L divergence between the probability distribution of a reference shallow moonquake P(x) and the probability distribution of the signal that we wish to categorize, Q(x), is given by:

$$K - L(P||Q) = \sum P(x) \frac{\log(P(x))}{Q(x)}. \quad (1)$$

The Kullback-Leibler (K-L) divergence measures how different two probability distributions are. It is always zero or higher, where zero means the two distributions are identical, and larger values indicate greater differences.

In the context of our study, we compare seismic signals using K-L divergence. Based on the spectral characteristics (Figures 2 and 3), we expect shallow moonquakes to resemble each other and thus have low K-L divergence when compared among themselves. On the other hand, impacts are expected to have different spectral characteristics from shallow moonquakes and, therefore, exhibit higher K-L divergence when compared to shallow moonquakes.

We compute the K-L divergence between each event and each known shallow moonquake in our data set, doing this separately for each station. For example, the data set at S14 contains 91 events, 86 impact events, and five shallow moonquake events (plotted in Figure S3 in Supporting Information S1), so there are five K-L comparisons. The average of these K-L comparisons measures how similar an individual signal is to the shallow moonquakes.

Since the data set at each station contains only a limited number of shallow moonquakes, we use a bootstrapping approach to prevent any single comparison from dominating the results. The bootstrapping process works as follows:

1. We repeatedly create new data sets by randomly resampling with replacement of the list of shallow moonquakes.
2. For each resampled data set, we compute the K-L divergence between the target event and each moonquake in the set and then average these values.

This process results in 1,000 average K-L divergence values for each target event. A low mean K-L divergence would suggest an event is similar in spectral shape and frequency content to the previously cataloged shallow events.

2.2.1. Distribution of K-L Divergence Values

We then look at the distributions of the 1,000 average K-L divergence values for each event, split into the two different types of events; shallow moonquakes and impacts. Figure 4 shows the two distributions for events recorded at stations S14, S15 and S16. For example, in Figure 4a, in orange is the distribution of 1,000 mean K-L values for each of the five shallow moonquakes contained within the station S14 data set, so 5,000 values in total. This orange distribution represents the similarity of shallow moonquakes to themselves. In blue is the distribution of the 1,000 mean K-L values for each of the 86 impacts within the station S14 data set, so 86,000 points in total—this blue distribution represents the similarity of shallow moonquakes to impacts.

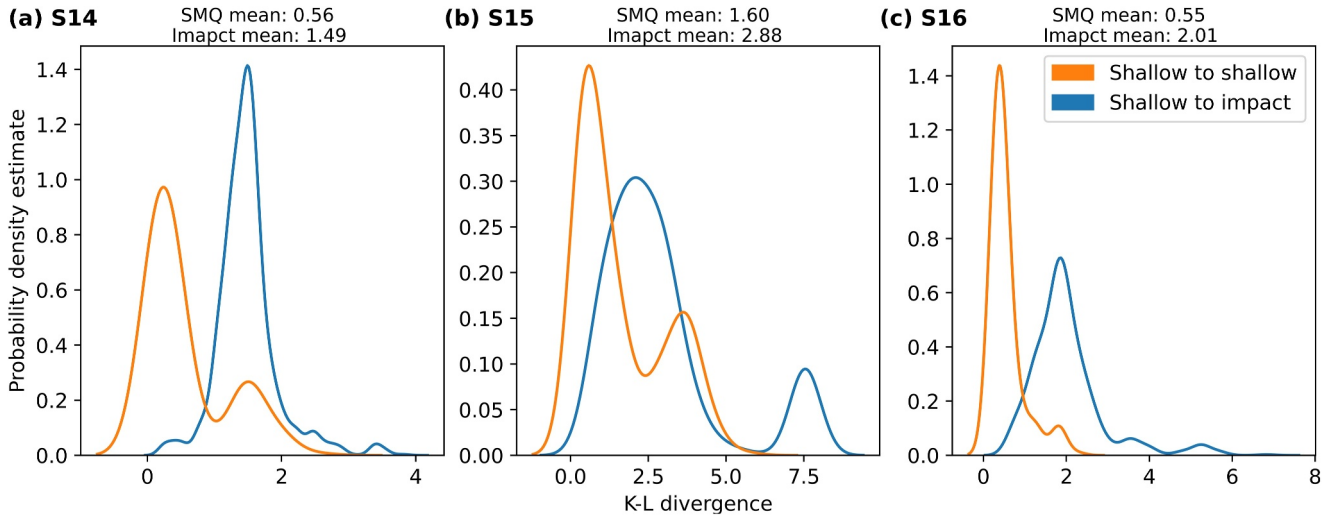

Figure 4. Smoothed distribution of Kullback-Leibler (K-L) divergence values calculated for waveforms recorded at (a) station S14, (b) station S15 and (c) station S16. The orange distribution is the bootstrapped K-L divergence values calculated from comparing shallow moonquakes to other cataloged shallow moonquakes. The blue distribution is the bootstrapped K-L divergence values calculated from comparing impacts to the cataloged shallow moonquakes. The lower K-L divergence between shallow moonquakes suggests that these are more similar to other events of the same class than they are to impacts.

The median value of the two distributions is displayed at the top of each panel. For the events recorded at station S14 (Figure 4a), the average similarity between shallow moonquakes and other shallow moonquakes is 0.56, while the average similarity between impacts and shallow moonquakes is 1.49. The lower mean K-L divergence value for the comparison between shallow moonquakes suggests that the spectra of shallow moonquakes are more similar to other shallow moonquakes than these are to impacts.

Similar distributions are observed when we consider the data sets of events recorded at stations S15 and S16 (Figures 4b and 4c) The data set at S15 contains 39 events: 6 shallow moonquakes and 33 impacts (plotted in Figure S4 in Supporting Information S1). The average similarity between shallow moonquakes and other shallow moonquakes is 1.60, while the average similarity between shallow moonquakes and impacts is 2.88. There is more overlap between the two distributions at station S15. The data set at S16 contains 41 events: 4 shallow moonquakes and 37 impacts (plotted in Figure S5 in Supporting Information S1). The average similarity between shallow moonquakes and other shallow moonquakes is 0.55, while the average similarity between shallow moonquakes and impacts is 2.01. At all the stations, the comparison between shallow moonquakes results in a lower average K-L divergence value, and the spectrograms of shallow moonquakes are more similar to those of other shallow moonquakes than those of impacts.

At all stations, the shallow moonquake distributions shown in orange have a second peak—a few shallow moonquakes look different to the rest. The higher K-L divergence compared to other shallow moonquakes may indicate a misclassified event but may also be due to differences in the signal quality or glitches that remain in the signal that make the signal appear different. For example, a shallow moonquake recorded at Station S15 on 23rd February 1974 contains high amplitude spikes, even after the despiking process. If we exclude this event from our analysis, we see that the second peak is reduced (Figure S6 in Supporting Information S1). This highlights the importance of pre-processing and smoothing to reduce the differences between events. We choose to present the full distribution, including the event on 23rd February 1974, to better represent the true uncertainty of the comparison under real data conditions.

It is important to note that the K-L divergence is not symmetrical; swapping P and Q in Equation 1, that is, using impact events as references, would lead to different K-L values for each event but yield similar overall comparison results for the whole population (see Figure S7 in Supporting Information S1).

Although there is an overlap between the distributions, we find that the spectral shapes and content of shallow moonquakes are distinct from those of impacts.

3. Time Domain Features of Lunar Seismic Signals

The analysis using the new K-L divergence metric allows us to compare the full spectra of two events to provide a guide of how similar they are but does not give details of the properties of the two populations of events beyond similarity. Instead of carrying out a pairwise comparison, another approach is to analyze individual events and identify the features that are different between the two populations of events. Here, we analyze each of the short-period seismograms of shallow moonquakes and impacts using the algorithms from tsfresh python package (Christ et al., 2018), and determine statistical metrics of each of the waveforms.

3.1. Data Processing

The data processing steps are the same as those described in Section 2.1 and used in the K-L divergence analysis. The same despiking steps are taken, and the data are converted to velocity waveforms with a pre-filter of 1–13 Hz. The waveforms are then used in the statistical algorithms of tsfresh without further processing.

3.2. Tsfresh Algorithm

Tsfresh is a Python library used to extract and select statistical features of any time series (Christ et al., 2018). The package can quickly extract and explore almost 800 different time series features and assess the statistical significance for predicting the target for each feature. Applying this method, we calculate features for each waveform recorded at stations S14, S15 and S16. Then, using the waveform labels from the catalog (either shallow moonquake or impact), we aim to determine which of these 800 features calculated for each event significantly differ between shallow moonquakes and impacts. Finally, to identify metrics that could be used to distinguish shallow moonquakes, we focus on a subset of these features with a large gap between the distribution of shallow moonquakes and that of impacts—the feature has a unique range for each event type.

First, we analyze the 39 events recorded at station S15. We find 18 features calculated for each event that have a 99% probability of being drawn from different distributions (the features have a p-value of less than 0.01). Although these features have a high probability of being drawn from two separate distributions (shallow moonquakes and impacts), the overlap in feature values between these two distributions means that many of the features may not be sufficient to distinguish between the events. Instead, we consider the subset of features where possible values that the distributions may take will have little overlap. These features, plotted in Figure 4, include:

- CID (Complexity Invariant Distance) estimate for a time series complexity (Figure 5a)—a measure of the number of peaks, valleys and features (Batista et al., 2014). We may expect shallow moonquakes to have a higher CID as shallow moonquakes are commonly observed to have two packets of seismic energy—a scattered P arrival and a scattered S arrival, as can be seen in Figure 2.
- Autocorrelation (Figure 5b)—the similarity of a signal to itself at an earlier time. Autocorrelation provides an indirect way to analyze the frequency content of a signal. A strong autocorrelation at a certain lag would suggest higher power in those frequencies. Comparing the autocorrelation at different lags between shallow moonquakes and impacts highlights the power in different frequency bands of the two signals.
- The skew of the absolute values of the Fourier transform spectra (Figure 5c)—a measure of the symmetry of the spectra and indicates differences in the shape of the spectra of the two classes, such as shallow moonquakes exciting a wider range of frequencies in the short period data. Note that while Figure 1 shows the spectra of shallow moonquakes and impacts, it shows a different frequency band than used in this tsfresh analysis.
- Spectral entropy (Figure 5d)—a measure of the spectral power distribution. If the signal's power is concentrated in just a few frequencies, the entropy will be low. If the power is spread out across many frequencies, the entropy will be high. We may expect shallow moonquakes to have a higher spectral entropy, as these excite a wider range of frequencies.

The features in Figure 5 are all directly or indirectly related to the signal's frequency content. For example, the autocorrelation shows you the periodicities of the entire waveform, and the power spectral density can be obtained from the Fourier transform of the autocorrelation function (Wiener, 1949). The direct relationship of the features to the frequency content reinforces the idea that the most apparent differences between shallow moonquakes and impacts can be observed in the frequency space.

Just as with the K-L divergence analysis, we also carry out the same time-domain analysis on the waveforms recorded at station S14 and S16. Figures S8 and S9 in Supporting Information S1 shows features at stations S14

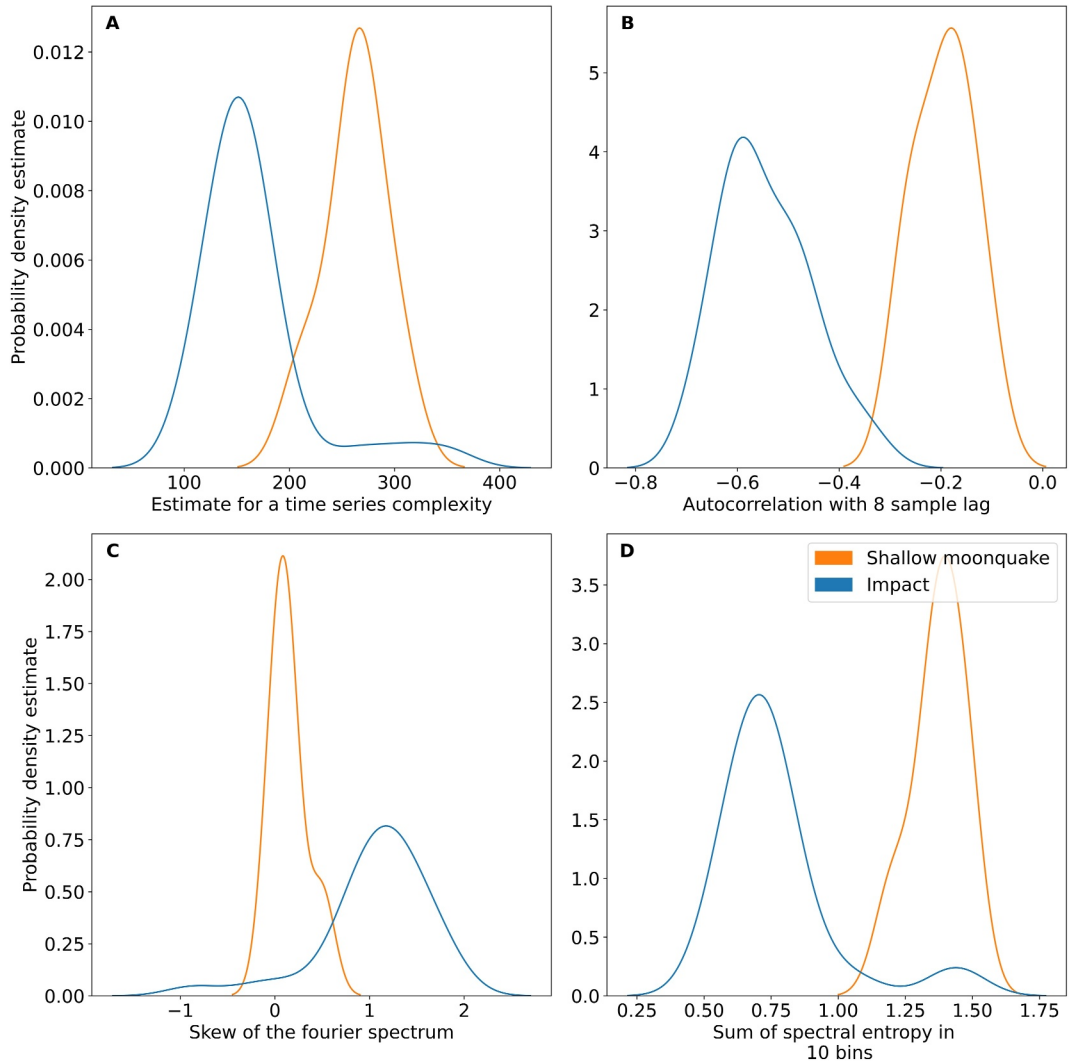

Figure 5. Example of four time-series features calculated from the 6 shallow moonquakes and 33 impacts recorded at station S15. The values calculated for each feature for impacts are plotted in blue and the values calculated for each feature for shallow moonquakes are plotted in orange. In each panel, the two distributions are different with 99% confidence. The features plotted are: (a) Complexity Invariant Distance Estimate for a time series complexity, a measure of the number of peaks, valleys and features (Batista et al., 2014). (b) Autocorrelation, the similarity of a signal to itself at an earlier time. (c) The skew of the absolute values of the Fourier transform spectra, a measure of the symmetry of the spectra and indicates differences in the frequency content of the two signal classes. (d) Spectral entropy—a measure of the spectral power distribution.

and S16 that are significantly different between impact waveforms and shallow moonquakes with 99% confidence. The distributions determined using events recorded at station S16 are visually separated and similar to those seen at station S15. The distributions of features determined from events recorded at station S14 are less easily separated—there is more overlap between the orange and blue distributions. We speculate that this may be because of the larger number of impacts included in the data set (>80, nearly double the data sets at S15 and S16), which could increase the variability of the impact signals. The influence of the size of the data set is further explored in Section 4.

4. Testing for Bias in Analysis

Our analysis suggests that both the K-L divergence and statistical metrics calculated from the waveform using the tsfresh algorithm can be used to distinguish shallow moonquakes from impacts. Recovering similar results with two independent methods (K-L divergence and tsfresh), and across events recorded at 3 different stations provides

confidence in the methods presented. However, for the K-L divergence comparison or tsfresh metrics to be useful for the re-analysis of Apollo seismic data or future lunar seismic data sets, we carry out further tests for bias in the methods and test how to generalize to other data sets. The full details of the tests for magnitude, distance and number of events are described in Supporting Information S1.

First, we test that the statistical metrics calculated for each event do not depend on the magnitude of the event. We find that the data set of events recorded at station S15 contains both large and small-magnitude shallow moonquakes and impacts, and as shown in Figure S10 in Supporting Information S1, there is no clear trend between metrics and the magnitude, which suggests that the features are not only dependent on the magnitude of the event.

Next, we test that the features do not solely reflect the event's distance from the station, using distance estimate is available from Nakamura et al., 1979 and Lognonné et al. (2003). The values of the features for impacts and shallow moonquakes have different values regardless of distance (Figure S10 in Supporting Information S1), suggesting that this feature depends on the source, not the distance.

It is important to note that the data sets at all the station are unbalanced—there are many more cataloged impacts than shallow moonquakes—in fact, it is the lack of shallow moonquakes that both motivates this work and makes the problem of distinguishing shallow moonquakes from impact events unsuitable for many machine-learning classification methods (due to the need for a robust training data set). However, we still want to check that the uneven data set and small sample of shallow moonquakes do not influence our results. To do so, we calculate the probability that the observed autocorrelation values for shallow moonquakes and impacts could arise from the same underlying distribution, reducing the number of events that we use to calculate the probability each time. We then repeat this 1,000 times, randomly perturbing the order for which the events are removed—a similar process to the bootstrapping described in Section 2.2. Figure S11 in Supporting Information S1 shows how the probability (or p-value) as a function of number events. A low p-value would suggest a high probability that the distribution of shallow moonquakes and impacts are different. There is still a 90% probability that the two distributions are different when there are only 10 events in the data set. The 10 events are 2 or 3 shallow moonquakes and 7 or 8 impacts. This suggests that the data sets we use for S14, S15 and S16, with at least 4 shallow moonquakes and $\geq$30 impacts, are statistically significant.

5. Z Events

In addition to events classified as shallow moonquakes or impacts in the original Nakamura et al. (1981) catalog, 250 events were assigned the classification "Z"—a mostly short-period event. These events have high amplitude signals recorded on the short-period instrument and could, therefore, possibly be shallow moonquakes that were not originally classified as such. We note that these events are inherently challenging to classify, having no distinct features of one class or another that were visible by eye, and that is why they were not classified originally.

To test this possibility, we first apply the K-L divergence method described in Section 1—comparing the overall spectral shape and frequency content of the Z events to the spectral shape of known shallow moonquakes. In this analysis, we consider 40 of the Z events recorded at station S15 as possible shallow moonquakes. The waveforms of these events are plotted in Figure S12 in Supporting Information S1. We only consider a small number of the Z events as many of the windows contain the signal of multiple events. The selected candidate events have a high signal-to-noise and a single event in the analysis window and are processed in the same way as described in Section 2.1.

Figure 6 shows the distribution of K-L divergence values for the population of Z events—a measure of the similarity of the shape and frequency content of the Z events to previous shallow moonquakes. None of the new Z events have low K-L values—they are all above 1 on average. This can be interpreted as the spectral shape and frequency content of the Z events being different to those of the previously cataloged moonquakes. The dissimilarity does not totally rule these events out as new shallow moonquakes—just that they look different to previously identified events, which could be due to many reasons such as data quality or source properties, which we discuss more in Section 7.

Next, we calculate the tsfresh features of the Z events, following the same procedure as described in Section 3.1. We calculate the CID, autocorrelation, skew of the Fourier spectra and the spectral density for the Z events and compare them to the values calculated for the cataloged shallow moonquakes and impacts.

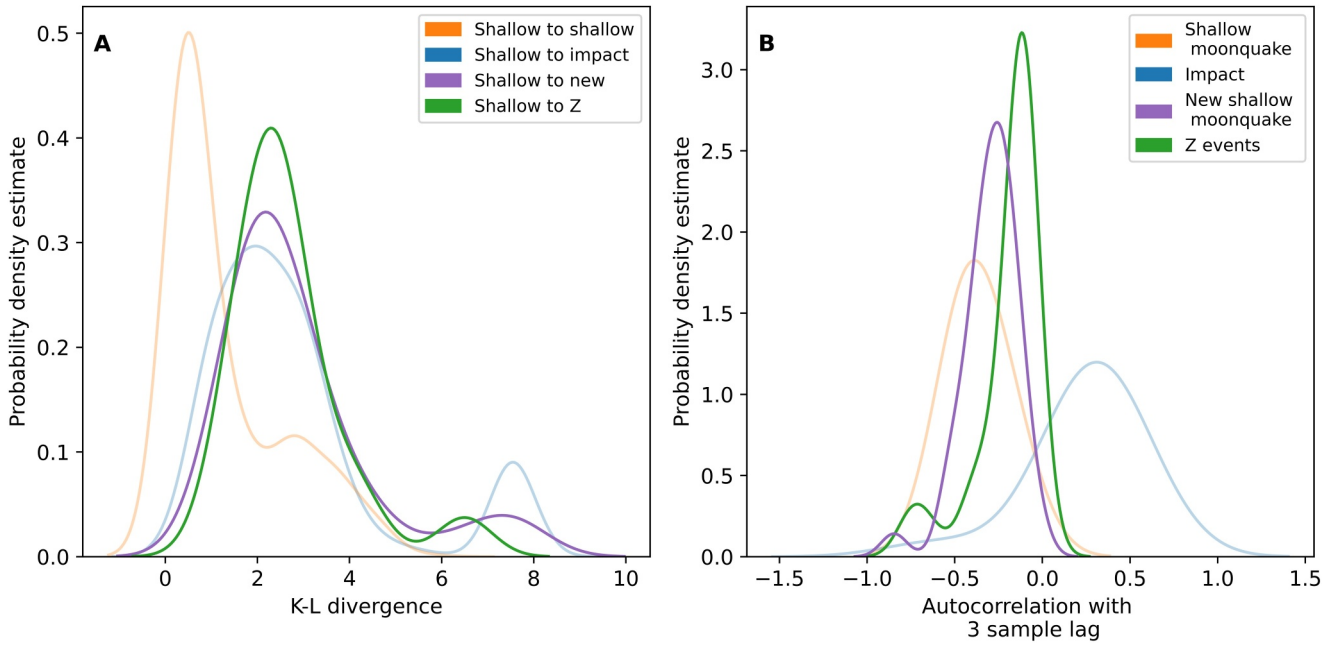

Figure 6. (a) Smoothed distribution of calculated Kullback-Leibler (K-L) divergence values calculated for waveforms recorded at station S15. The orange distribution is the bootstrapped K-L divergence values calculated from comparing shallow moonquakes to other cataloged shallow moonquakes and is the same as plotted in Figure 4b. The blue distribution is the bootstrapped K-L divergence values calculated from comparing impacts to the cataloged shallow moonquakes and is the same as plotted in Figure 4b. The green distribution is the bootstrapped K-L divergence values calculated from comparing Z events to previously cataloged shallow moonquakes. The purple distribution is the K-L divergence values calculated from comparing (Onodera, 2024) shallow moonquakes to previously cataloged shallow moonquakes. (b) Example of the autocorrelation values calculated for the same 4 sets of events.

Figure 6b shows an example of the autocorrelation values calculated for the previously identified shallow moonquakes and impacts (in orange and blue respectively), and the new Z events in green. In the distributions the Z events overlap with both the shallow moonquakes and impacts, suggesting a variety in the signal characteristics of the group. Perhaps some are shallow moonquakes, and some are impacts.

Another way of presenting the tsfresh results is shown in Figure 7. Figure 7 shows a pair plot, where each of the four features from Figure 5 (CID, autocorrelation, Fourier skew and spectral entropy) are plotted against one another. The diagonal elements show the univariate KDE for each feature, the same as Figure 5, with the addition of the distributions for the Z events shown in Green. Again, just as was shown in the autocorrelation example in Figure 6b, the distribution of Z events overlaps with both shallow moonquakes and impacts.

These diagonal panels that show the univariate KDE estimates is not the clearest way to represent this when we would like to analyze individual events in the population. Instead, we can look at the pair-wise distributions, plotted in the off-diagonals in Figure 7. Each of these plots one feature against another, with each event shown by colored circles. In these plots we can see that the Z-events seem to fall on a spectrum between the clusters for shallow moonquakes and impacts—many seem to fall closer to the cluster of impacts, but one or two are very close to the small cluster of orange shallow moonquake dots.

Since the values of each of the features for the Z events seem to plot somewhere between shallow moonquakes and impacts, we quantify a linear mixing fraction, f;

$$f = \frac{(Q_{test} - Q_{SMQmean})}{(Q_{impactmean} - Q_{SMQmean})}, \quad (2)$$

where Q_{test}, is the value of the feature for each of the Z events of interest, $Q_{SMQmean}$ is the mean value of the feature for all of the previously cataloged shallow moonquakes, and $Q_{impactmean}$ is the mean value of the feature for impacts. This linear mixing fraction describes how far along the line joining $Q_{SMQmean}$ and $Q_{impactmean}$ a point lies. We calculate this value for each of the four tsfresh features, CID, autocorrelation, the skew of the Fourier spectra,

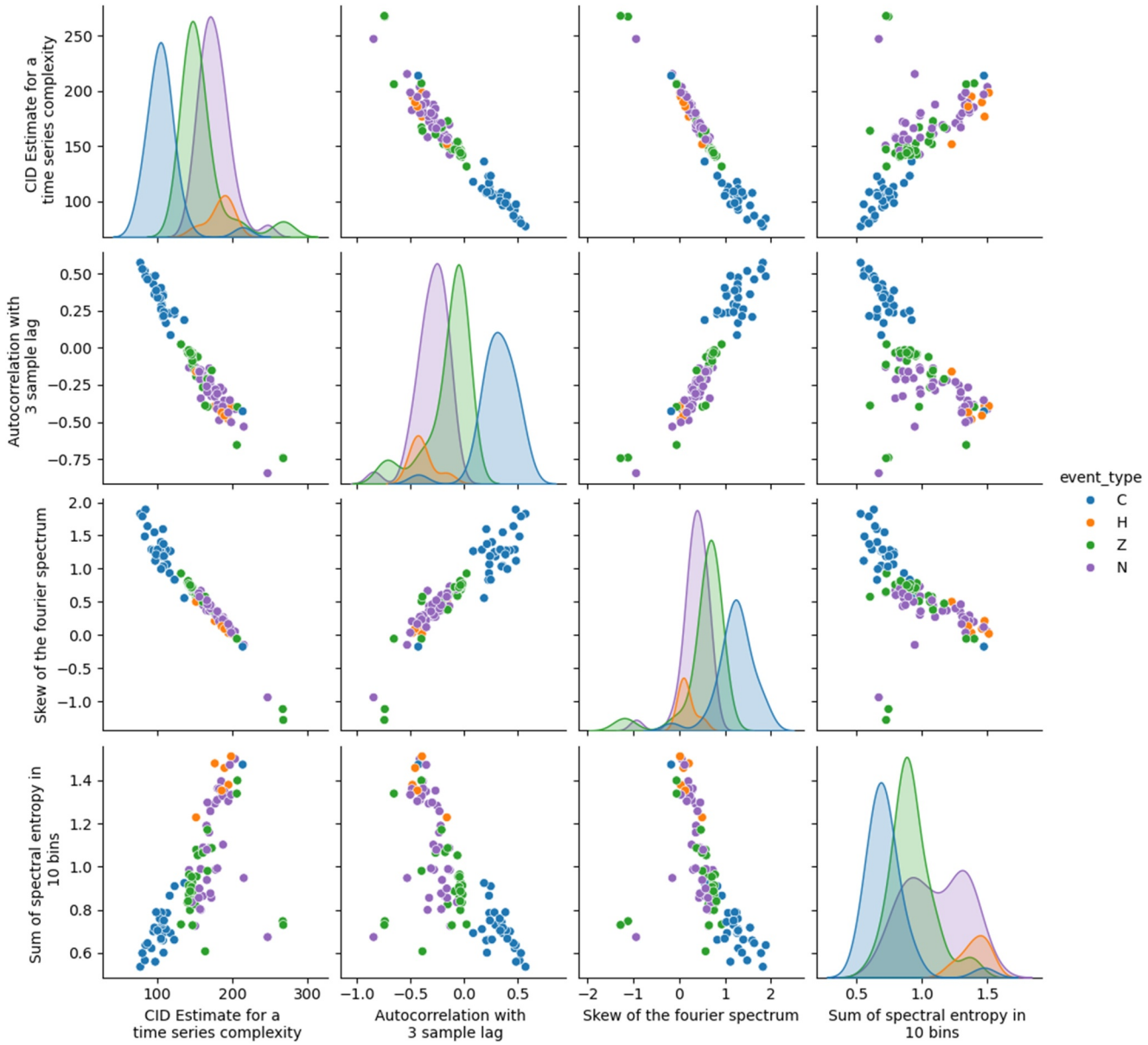

Figure 7. Example of four time-series features calculated from the 6 shallow moonquakes (H), 33 impacts (C), 40 Z-events (Z) and 40 new shallow moonquakes (N) recorded at station S15. Shallow moonquakes are plotted in orange, impacts in blue, Z-events in green and new shallow moonquakes identified by (Onodera, 2024) in purple. The features plotted are: CID Estimate for a time series complexity, a measure of the number of peaks, valleys and features (Batista et al., 2014); Autocorrelation, the similarity of a signal to itself at an earlier time; The skew of the absolute values of the Fourier transform spectra, a measure of the symmetry of the spectra and indicates differences in the frequency content of the two signal classes and Spectral entropy—a measure of the spectral power distribution. The diagonal distributions for each figure are equivalent to Figure 5, with the addition of the green and purple distributions for Z-events and new shallow moonquakes, respectively. However, for Z events and new moonquakes, we may wish to examine the values for individual events. The off-diagonal panels show scatter plots of pairs of features, where individual events are plotted as colored circles.

and spectral entropy. For each Z event, we sum the four fractions and divide by 4 to get an overall fraction across the four features. This "total mixing fraction" can vary between −1 and 1, with negative values implying the point falls out of the bounds of impacts and shallow moonquakes. If a Z event falls close to the cluster of shallow moonquakes in all four features, it will have a total mixing fraction close to 0. If the Z event instead falls closer to the cluster of impacts, it will have a larger total mixing fraction.

The tsfresh values and mixing fractions are tabulated in Table S1. Most of the Z events have a total mixing fraction ≥0.5, suggesting that these events are more similar to impacts than shallow moonquakes. However, one

event on 1975-01-20 at 05:28 a.m. has a total mixing fraction of just −0.14. The time series and spectra of this event are plotted in Figure S13 in Supporting Information S1. No clear P or S arrival can be seen in the time series, just a long emergent arrival which reaches a maximum just before 200 s after the start of the signal. This more emergent arrival is visually similar to other cataloged shallow moonquakes (e.g., the shallow moonquake recorded on station S15 1973-03-13, Figure S4 in Supporting Information S1). The signal has frequencies above 10 Hz and no decay in frequencies with time. This event could be another shallow moonquake.

6. New Shallow Moonquakes

So far in this study we have focused our analysis on testing events previously identified and recorded in the original Nakamura et al. (1981) catalog. However, over 40 new shallow moonquakes were recently identified and quantitatively classified from the short-period seismic data by Onodera (2024), resulting in a new b-value estimate including the new events of 0.8 (an increase from 0.5 determined using events from the Nakamura et al. (1981) catalog). Onodera (2024) identified new events in the continuous day traces by computing the coherence of the spectral density between data segments and a template shallow moonquake. Segments with calculated coherence ≥0.6 were flagged as possible new seismic events. Although a coherence approach was used to identify possible new events, the events were categorized into thermal moonquakes, impacts and shallow moonquakes based on visual interpretation. In fact, the high coherence found in the Onodera (2024) study between impacts and target shallow moonquakes re-iterates the similarity between these signals and the need for a quantitative method to distinguish source types. Impact signals in his study were qualitatively categorized based on the long duration (≥10–15 min) and monatomic energy decay at high frequencies. In contrast, shallow moonquakes were qualitatively categorized based on two packets of energy (P- and S-wave arrivals) and energy excitation of 2–8 Hz or higher.

6.1. Statistical Analysis of Newly Identified Shallow Moonquakes

As a further test of our method, we analyzed these qualitatively classified events using our statistical metrics– K-L divergence and tsfresh. We took the new events from the supplementary information of Onodera (2024), and downloaded the data segments recorded on the S15 station. The events were processed in the same way as outlined in Sections 2.1 and 3.1 and plotted in Figure S14 in Supporting Information S1. The waveforms are of lower quality, more similar in appearance to the more transitional Z events. Using these waveforms, we determined the kernel density estimates and calculated the pairwise K-L divergence. The comparison of new shallow moonquakes to originally cataloged shallow moonquakes is Figure 6a in purple. Similar to the Z events, the newly identified shallow moonquakes have an average K-L divergence value above 1. Again, this may indicate that the K-L divergence may be more effective at distinguishing high-quality events.

Next, we calculated the tsfresh features found to be significant for the original shallow moonquakes. In addition to the tsfresh values for the Z events shown in green, Figure 7 shows a pair plot, where each of the four features from Figure 5 (CID, autocorrelation, Fourier skew and spectral entropy) are plotted against one another, where the new moonquakes are plotted in purple. The diagonal elements show the univariate KDE for each feature; the purple distributions for the shallow moonquakes mostly overlap with the distribution of previously identified shallow moonquakes, plotted in orange, but some events do overlap with the distribution of impacts shown in blue—especially in the distributions for the spectral entropy. We can look at the pair-wise distributions, plotted in the off-diagonals in Figure 7. Each of these plots one feature against another, with each of the new shallow moonquakes plotted in purple. Similar to the Z events, the new moonquakes seem to fall on a spectrum between the clusters for shallow moonquakes and impacts.

Finally, we also calculate the total mixing fraction for the new shallow moonquakes. 50% of the new shallow moonquakes have a mixing fraction of less than 0.2, suggesting that they are similar to the previously cataloged shallow moonquakes, and we have high confidence in the identification of these new events. The higher fraction for the other events does not rule out that they are shallow moonquakes, but may be used to flag these events less similar to previously identified events. Including this information in future catalogs as a quantitative way to describe the confidence in an event may be useful for future users of the catalog.

7. Implications for Lunar Tectonics

7.1. Updated B-Value Estimate

As discussed in the introduction, tectonic earthquakes have a Gutenberg–Richter distribution with a slope (or b-value) of 1 on Earth. On the Moon, the b-value using only the 28 original shallow moonquakes is only 0.5 (Nakamura, 1977, 1980). Onodera (2024) determined a new b-value estimate, including all the new shallow moonquake events, of 0.8. However, from our analysis we find that some events are less similar to previous events, and we may have less confidence in the classification. We, therefore, recalculate the b-value using the subset of events that fall very close to the previously cataloged events.

Like Onodera (2024), we estimate the magnitude of completeness M_c, the b-value, using the maximum likelihood technique developed by Aki (1965), implemented in Python by Lapins (2021). We find that using only the new shallow moonquakes with a low total mixing fraction leads to a magnitude of completeness of M_b 5 and a b-value of 0.77 ± 0.1 within the uncertainty of Onodera (2024) updated estimate.

It is important to note that the uncertainty quoted above likely underestimates the true uncertainty in our lunar b-value estimation. The b-value was calculated with only a small number of events across a limited magnitude range; hundreds, if not thousands, of events over several orders of dynamic range, would be needed to more accurately estimate a lunar b-value (e.g., Okal & Romanowicz, 1994; Roberts et al., 2015). Another important consideration is the uncertainty of the magnitudes used to estimate the b-value. Here, we have used the minimum body wave magnitudes calculated by Onodera (2024). Empirical corrections are used to correct the moonquakes' displacement spectrum because of the uncertainties in factors such as the source location, radiation pattern and site amplification.

The estimate of the b-value of 0.7 is slightly lower than the Earth's average of around one, but wide-ranging b-values ($0.3 \leq b \leq 2.5$) have been reported in the literature (e.g., El-Isa & Eaton, 2014). Interpreting physical processes associated with particular b-value remains contentious and have been attributed to prevailing stress state (e.g.., C. Scholz, 1968; C. H. Scholz, 2015), crustal heterogeneity (e.g., Mori & Abercrombie, 1997), pore pressure (e.g., Wyss et al., 1997), geothermal gradient (e.g., Warren & Latham, 1970) or tectonic setting (e.g.., Frohlich & Davis, 1993; Schorlemmer et al., 2005). Onodera (2024) use a b-value of 0.7 as one piece of evidence to indicate a moderately heterogeneous source region of shallow moonquakes, and place shallow moonquake depths below the highly heterogeneous scattering layer. Here, we do not identify any particular cause for the b-value of ∼0.7; we highlight the caution in interpreting the b-value in terms of the geological setting without other lines of geophysical evidence, especially given the high uncertainty. Other methods, for example, evidence from coda wave scattering (Blanchette-Guertin et al., 2012; Gillet et al., 2017; Onodera, 2024), or direct depth estimation would be better suited for placing shallow moonquakes in or below the scattering layer.

7.2. Depth Distribution of Shallow Moonquakes

Our analysis shows that all of the classes of events—impacts, cataloged shallow moonquakes, Z events and newly identified shallow moonquakes show a range of properties. In particular, the Z and Onodera (2024)'s newly identified shallow moonquakes fall on a spectrum between the impacts and cataloged shallow moonquakes. Here, we present possible reasons why there is such a range of time series and spectral content, particularly for the Z and newly identified shallow moonquakes.

A large fraction of the variability in the signals can be attributed to (a) the epicentral distance, (b) the magnitude of the event or (c) the signal-to-noise ratio (which also depends on the first two factors). The epicentral distance, magnitude and maximum STA/LTA as a function of the total mixing fraction for the new moonquakes identified by Onodera (2024) can be seen in Figure S15 in Supporting Information S1. To account for this dependence, we normalize the total mixing fraction using a reference distance of 2,000 km, a reference minimum body wave magnitude of 4.8 and a reference maximum STA/LTA of 3 (panel d).

However, even when correcting for the estimated distance and magnitude of the event, there is still considerable variability in the signal. A simple explanation for the variability that we see would be that there may be more variability in shallow moonquakes' source depths than previously thought. This could particularly explain why

some shallow moonquakes have more impulsive P and S arrivals, while others seem to have very emergent arrivals for both the P and the S—shallower source depths with more scattering may lead to more emergent arrivals.

8. Application to Future Lunar Seismic Data

In this work, we have presented various statistical methods to support the classification of lunar seismic events. In this section, we discuss the advantages and disadvantages of these methods and how they may be applied to data from future lunar missions.

Previous studies on the lunar seismic data have classified events based on qualitative visual inspection of the spectral content and arrivals. However, this is time-consuming and challenging. By taking advantage of the detailed work done to previously catalog events, we can find quantitative and physically meaningful metrics related to different kinds of lunar seismic events. We also introduce the "mixing fraction"—a metric that quantifies the similarity between a new event and the previously identified shallow moonquakes. The differences between signals, quantified by the mixing fraction, can represent differences in event distance, data quality and depth. Since the mixing value places an event on a spectrum between shallow moonquake and impact, it can also indicate confidence in classification, with high confidence in new events that are very similar to previously classified events.

We acknowledge that the metrics are not perfect—there is still overlap in the distributions between shallow moonquakes and impacts, in particular for the K-L divergence. The distributions are influenced by local site effects and vary between stations, and they currently cannot deal with low signal-to-noise events or multiple events within an analysis window. However, the K-L divergence and time series analysis, used in combination with visual analysis, can flag possible event types and guide decision-making processes with quantitative metrics.

Developing new methods and workflows to distinguish and catalog seismic events represents key preparation for the upcoming lunar seismic data collection in the next decade. Planned future missions include the Farside Seismic Suite (FSS),the Lunar Environment Monitoring Station (LEMS) and China's Chang'e 7 and 8 missions. The new generation of lunar seismic instruments will have higher digitization than the Apollo instrument. The instruments will also be more sensitive than the Apollo-era seismic instruments—the FSS very broadband seismometer (VBB) will be the most sensitive ever in the sensing range of 0.1–1 Hz, but with more limited improvements in sensitivity on the VBB and short-period instrument at the higher frequencies important for shallow moonquakes and impacts (Aboobaker et al., 2024). Even with improvements in instrumentation, the challenges in discriminating signals will persist. The observed lunar seismic waveforms will be highly scattered due to the nature of the lunar crust and, therefore, are likely to have similar characteristics to those recorded on the Apollo instruments. Finally, the operation period of these instruments will be much shorter than the Apollo seismic network, which will limit the number of observed signals, particularly rare shallow moonquakes.

It is likely that the signals observed by new instruments will be characteristically similar to events recorded on the Apollo instruments. We advocate adopting and adapting these quantitative classification methods for future lunar data, as they take advantage of and build upon the knowledge of Apollo seismic data. Quantitative metrics will provide a basis for classifying events and give additional information to catalog users about confidence in classifications.

9. Conclusion

In this work, we set out to quantify the distinctions between shallow moonquakes and impacts, as previous studies have relied on qualitative differences in frequency content to classify lunar seismic events. We compared the spectra of shallow moonquakes to previously recorded shallow moonquakes and impacts using the K-L divergence. We found that the cataloged shallow moonquakes are more similar to other shallow moonquakes than they are to impacts. We also identified metrics using the tsfresh algorithm that could be used to classify events without directly comparing them to previous events. By analyzing the time series, we identified features related to the spectral content that significantly differ between shallow moonquakes and impacts. We then apply these same methods to previously identified but unclassified high frequency events and new moonquakes identified by Onodera (2024). One event within the unclassified high-frequency events may be a shallow moonquake. The majority of the new moonquakes identified by Onodera (2024) are quantitatively consistent with shallow moonquakes from the original catalog, validating a 40% increase in observed shallow lunar seismicity and an

increase in b-value from 0.5 to 0.7. The K-L divergence method is sensitive to the quality of the signals, while the tsfresh method is more flexible. The two methods in combination provide a quantitative way to distinguish between shallow moonquakes and impact events. We advocate for the use of quantitive metrics in the creation of catalogs of future lunar seismic events.

Data Availability Statement

All the Apollo seismic data were retrieved from EarthScope (formerly IRIS, Nunn, 1969). The lunar seismic catalog is available from Nakamura et al. (1981). The tsfresh algorithm is available from Christ et al., 2018, and implementation of the K-L diveregnce used the scikit-learn package (Pedregosa et al., 2011). Figures were prepared in Matplotlib (Hunter, 2007). A jupyter notebook containing a simple tutorial on applying the K-L divergence and tsfresh algorithms to the lunar seismic data can be found at Turner (2024).

Acknowledgments
We would like to thank the editor and two anonymous reviewers for thier helpful feedback that greatly improved the manuscript. We would like to thank Yosio Nakamura for his useful insights on the Apollo seismic data and helpful input on this manuscript. AT was supported by the University of Texas Insitute for Geophysics (UTIG) distinguished postdoctoral fellowship. This is University of Texas Institute for Geophysics (UTIG) Contribution 4037 and University of Texas Center for Planetary Systems Habitability (CPSH) Contribution 0089.

References

Aboobaker, A., Panning, M., & Bugby, D. (2024). The farside seismic suite: A novel approach for long-term lunar seismology. In *2024 IEEE aerospace conference* (pp. 1–8).

Aki, K. (1965). Maximum likelihood estimate of b in the formula log N= a-bM and its confidence limits. *Bulletin of the Earthquake Research Institute, University of Tokyo*, *43*, 237–239.

Aki, K., & Richards, P. G. (2002). Quantitative seismology.

Araki, H. (2001). Focal processes of deep moonquakes. *Journal of the Geodetic Society of Japan*, *47*(1), 508–513.

Batista, G. E. A. P. A., Keogh, E. J., Tataw, O. M., & De Souza, V. M. A. (2014). CID: An efficient complexity-invariant distance for time series. *Data Mining and Knowledge Discovery*, *28*(3), 634–669. https://doi.org/10.1007/s10618-013-0312-3

Beyreuther, M., Barsch, R., Krischer, L., Megies, T., Behr, Y., & Wassermann, J. (2010). ObsPy: A python toolbox for seismology. *Seismological Research Letters*, *81*(3), 530–533. https://doi.org/10.1785/gssrl.81.3.530

Blanchette-Guertin, J.-F., Johnson, C. L., & Lawrence, J. F. (2012). Investigation of scattering in lunar seismic coda. *Journal of Geophysical Research*, *117*(E6), 2011JE004042. https://doi.org/10.1029/2011JE004042

Borji, A. (2022). Pros and cons of GAN evaluation measures: New developments. *Computer Vision and Image Understanding*, *215*, 103329. https://doi.org/10.1016/j.cviu.2021.103329

Bulow, R. C., Johnson, C. L., Bills, B. G., & Shearer, P. M. (2007). Temporal and spatial properties of some deep moonquake clusters. *Journal of Geophysical Research*, *112*(E9), 2006JE002847. https://doi.org/10.1029/2006JE002847

Bulow, R. C., Johnson, C. L., & Shearer, P. M. (2005). New events discovered in the Apollo lunar seismic data. *Journal of Geophysical Research*, *110*(E10), 2005JE002414. https://doi.org/10.1029/2005JE002414

Christ, M., Braun, N., Neuffer, J., & Kempa-Liehr, A. W. (2018). Time series feature extraction on basis of scalable hypothesis tests (tsfresh–a python package) [Software]. *Neuro computing*, *307*, 72–77. https://doi.org/10.1016/j.neucom.2018.03.067

Civilini, F., Weber, R., & Husker, A. (2023). Thermal moonquake characterization and cataloging using frequency-based algorithms and stochastic gradient descent. *Journal of Geophysical Research: Planets*, *128*(9), e2022JE007704. https://doi.org/10.1029/2022JE007704

Daubar, I., Lognonné, P., Teanby, N. A., Miljkovic, K., Stevanović, J., Vaubaillon, J., et al. (2018). Impact-seismic investigations of the in sight mission. *Space Science Reviews*, *214*(8), 132. https://doi.org/10.1007/s11214-018-0562-x

Douglas, A. (2013). *Forensic seismology and nuclear test bans*. Cambridge University Press.

Duennebier, F., & Sutton, G. H. (1974a). Meteoroid impacts recorded by the short-period component of Apollo 14 lunar passive seismic station. *Journal of Geophysical Research*, *79*(29), 4365–4374. https://doi.org/10.1029/JB079i029p04365

Duennebier, F., & Sutton, G. H. (1974b). Thermal moonquakes. *Journal of Geophysical Research*, *79*(29), 4351–4363. https://doi.org/10.1029/JB079i029p04351

Edwards, W. N., Eaton, D. W., & Brown, P. G. (2008). Seismic observations of meteors: Coupling theory and observations. *Reviews of Geophysics*, *46*(4), 2007RG000253. https://doi.org/10.1029/2007RG000253

El-Isa, Z. H., & Eaton, D. W. (2014). Spatiotemporal variations in the b-value of earthquake magnitude–frequency distributions: Classification and causes. *Tectonophysics*, *615*, 1–11. https://doi.org/10.1016/j.tecto.2013.12.001

Frohlich, C., & Davis, S. D. (1993). Teleseismic b values; or, much ado about 1.0. *Journal of Geophysical Research*, *98*(B1), 631–644. https://doi.org/10.1029/92jb01891

Gillet, K., Margerin, L., Calvet, M., & Monnereau, M. (2017). Scattering attenuation profile of the moon: Implications for shallow moonquakes and the structure of the megaregolith. *Physics of the Earth and Planetary Interiors*, *262*, 28–40. https://doi.org/10.1016/j.pepi.2016.11.001

Gudkova, T., Lognonné, P., Miljković, K., & Gagnepain-Beyneix, J. (2015). Impact cutoff frequency–momentum scaling law inverted from Apollo seismic data. *Earth and Planetary Science Letters*, *427*, 57–65. https://doi.org/10.1016/j.epsl.2015.06.037

Gudkova, T., Lognonné, P. H., & Gagnepain-Beyneix, J. (2011). Large impacts detected by the Apollo seismometers: Impactor mass and source cutoff frequency estimations. *Icarus*, *211*(2), 1049–1065. https://doi.org/10.1016/j.icarus.2010.10.028

Hunter, J. D. (2007). Matplotlib: A 2D graphics environment [Software]. *Computing in Science & Engineering*, *9*(3), 90–95. https://doi.org/10.1109/mcse.2007.55

Knapmeyer-Endrun, B., & Hammer, C. (2015). Identification of new events in Apollo 16 lunar seismic data by hidden Markov Model-based event detection and classification. *Journal of Geophysical Research: Planets*, *120*(10), 1620–1645. https://doi.org/10.1002/2015JE004862

Koper, K. D., Burlacu, R., Murray, R., Baker, B., Tibi, R., & Mueen, A. (2024). Inferring the focal depths of small earthquakes in southern California using physics-based waveform features. *Bulletin of the Seismological Society of America*, *114*(5), 2376–2396. https://doi.org/10.1785/0120230307

Koyama, J., & Nakamura, Y. (1980). Focal mechanism of deep moonquakes. In *Lunar and planetary science conference, 11th, houston, tx, march 17-21, 1980, proceedings*. Pergamon Press, (Vol. 11, pp. 1855–1865).

Kullback, S., & Leibler, R. A. (1951). On information and sufficiency. *The Annals of Mathematical Statistics*, *22*(1), 79–86. https://doi.org/10.1214/aoms/1177729694

Lammlein, D. R., Latham, G. V., Dorman, J., Nakamura, Y., & Ewing, M. (1974). Lunar seismicity, structure, and tectonics. *Reviews of Geophysics*, *12*(1), 1–21. https://doi.org/10.1029/RG012i001p00001

Lapins, S. (2021). *Detecting and characterising seismicity associated with volcanic and magmatic processes through deep learning and the continuous wavelet transform*. University of Bristol.

Latham, G., Ewing, M., Dorman, J., Press, F., Toksoz, N., Sutton, G., et al. (1970). Seismic data from man-made impacts on the moon. *Science*, *170*(3958), 620–626. https://doi.org/10.1126/science.170.3958.620

Latham, G., Ewing, M., Press, F., & Sutton, G. (1969). The Apollo passive seismic experiment: The first lunar seismic experiment is described. *Science*, *165*(3890), 241–250. https://doi.org/10.1126/science.165.3890.241

Latham, G., Ewing, M., Press, F., Sutton, G., Dorman, J., Nakamura, Y., et al. (1970). Apollo 11 passive seismic experiment. In *Geochimica et cosmochimica acta supplement, volume 1. proceedings of the Apollo 11 lunar science conference held 5-8 January, 1970 in houston, tx. volume 2: Chemical and isotope analyses* (Vol. 1, p. 2309). aa levinson. New York: Pergammon Press, 1970.

Li, C., Wang, C., Wei, Y., & Lin, Y. (2019). China's present and future lunar exploration program. *Science*, *365*(6450), 238–239. https://doi.org/10.1126/science.aax9908

Lognonné, P., Gagnepain-Beyneix, J., & Chenet, H. (2003). A new seismic model of the moon: Implications for structure, thermal evolution and formation of the moon. *Earth and Planetary Science Letters*, *211*(1–2), 27–44. https://doi.org/10.1016/s0012-821x(03)00172-9

Maceira, M., Blom, P. S., MacCarthy, J. K., Marcillo, O. E., Euler, G. G., Begnaud, M. L., et al. (2017). *Trends in nuclear explosion monitoring research and development-a physics perspective (Technical Reports)*. Los Alamos National Lab.(LANL).

Mori, J., & Abercrombie, R. E. (1997). Depth dependence of earthquake frequency-magnitude distributions in California: Implications for rupture initiation. *Journal of Geophysical Research*, *102*(B7), 15081–15090. https://doi.org/10.1029/97jb01356

Nakamura, Y. (1977). HFT events: Shallow moonquakes? *Physics of the Earth and Planetary Interiors*, *14*(3), 217–223. https://doi.org/10.1016/0031-9201(77)90174-1

Nakamura, Y. (1980). Shallow moonquakes-how they compare with earthquakes. In *Lunar and planetary science conference, 11th, Houston, TX, March 17-21, 1980, proceedings*. Pergamon Press, (Vol. 11, pp. 1847–1853).

Nakamura, Y. (2003). New identification of deep moonquakes in the Apollo lunar seismic data. *Physics of the Earth and Planetary Interiors*, *139*(3–4), 197–205. https://doi.org/10.1016/j.pepi.2003.07.017

Nakamura, Y., Latham, G. V., Dorman, H. J., & Harris, J. (1981). Passive seismic experiment, long period event catalog, final version (1969 day 202-1977 day 273, alsep stations 11, 12, 13, 14, 15, and 16) [Dataset]. https://doi.org/10.15781/T2FF3MH78

Nakamura, Y., Latham, G. V., Dorman, H. J., Ibrahim, A.-B., Koyama, J., & Horvath, P. (1979). Shallow moonquakes-depth, distribution and implications as to the present state of the lunar interior. In In: *Lunar and planetary science conference, 10th, Houston, Tex., March 19-23, 1979, proceedings*. Pergamon Press, Inc., (Vol. 10, pp. 2299–2309).

Nunn, C. (1969). Apollo passive seismic experiments [Dataset]. *International Federation of Digital Seismograph Networks*. https://doi.org/10.7914/SN/XA_1969

Nunn, C., Fernando, B. A., & Panning, M. P. (2024). Artificial impacts on the moon: Modeling 3d seismic propagation effects with axisem3d. *The Planetary Science Journal*, *5*(11), 246. https://doi.org/10.3847/psj/ad83d2

Nunn, C., Garcia, R. F., Nakamura, Y., Marusiak, A. G., Kawamura, T., Sun, D., et al. (2020). Lunar seismology: A data and instrumentation review. *Space Science Reviews*, *216*(5), 89. https://doi.org/10.1007/s11214-020-00709-3

Nunn, C., Nakamura, Y., Kedar, S., & Panning, M. P. (2022). A new archive of Apollo's lunar seismic data. *The Planetary Science Journal*, *3*(9), 219. https://doi.org/10.3847/psj/ac87af

Okal, E. A., & Romanowicz, B. A. (1994). On the variation of b-values with earthquake size. *Physics of the Earth and Planetary Interiors*, *87*(1–2), 55–76. https://doi.org/10.1016/0031-9201(94)90021-3

Onodera, K. (2024). New views of lunar seismicity brought by analysis of newly discovered moonquakes in apollo short-period seismic data. *Journal of Geophysical Research: Planets*, *129*(7), e2023JE008153. https://doi.org/10.1029/2023JE008153

Onodera, K., Kawamura, T., Tanaka, S., Ishihara, Y., & Maeda, T. (2022). Quantitative evaluation of the lunar seismic scattering and comparison between the Earth, Mars, and the moon. *Journal of Geophysical Research: Planets*, *127*(12), e2022JE007558. https://doi.org/10.1029/2022JE007558

Panning, M., Kedar, S., Bowles, N., Bugby, D., Calcutt, S., Cutler, J., et al. (2022). Farside seismic suite (fss): Surviving the lunar night and delivering the first seismic data from the farside of the moon. In *53rd lunar and planetary science conference* (Vol. 2678).1576.

Pedregosa, F., Varoquaux, G., Gramfort, A., Michel, V., Thirion, B., Grisel, O., et al. (2011). Scikit-learn: Machine learning in python [Software] [Dataset]. *Journal of Machine Learning Research*, *12*, 2825–2830. Retrieved from https://scikit-learn.org/

Roberts, N. S., Bell, A. F., & Main, I. G. (2015). Are volcanic seismic b-values high, and if so when? *Journal of Volcanology and Geothermal Research*, *308*, 127–141. https://doi.org/10.1016/j.jvolgeores.2015.10.021

Salimans, T., Goodfellow, I., Zaremba, W., Cheung, V., Radford, A., & Chen, X. (2016). Improved techniques for training gans. *Advances in Neural Information Processing Systems*, *29*.

Schmerr, N., Benna, M., McCall, N., Bailey, S., DellaGiustina, D., Bray, V., et al. (2024). The lunar environmental monitoring station: An artemis 3 deployed instrument. *LPI Contributions*, *3060*, 6010.

Scholz, C. (1968). The frequency-magnitude relation of microfracturing in rock and its relation to earthquakes. *Bulletin of the Seismological Society of America*, *58*(1), 399–415. https://doi.org/10.1785/bssa0580010399

Scholz, C. H. (2015). On the stress dependence of the earthquake b value. *Geophysical Research Letters*, *42*(5), 1399–1402. https://doi.org/10.1002/2014gl062863

Schorlemmer, D., Wiemer, S., & Wyss, M. (2005). Variations in earthquake-size distribution across different stress regimes. *Nature*, *437*(7058), 539–542. https://doi.org/10.1038/nature04094

Shearer, P. M. (2019). *Introduction to seismology*. Cambridge University Press.

Stein, S., & Wysession, M. (2009). *An introduction to seismology, earthquakes, and earth structure*. John Wiley & Sons.

Thurin, J., Tape, C., & Modrak, R. (2022). Multi-event explosive seismic source for the 2022 m w 6.3 hunga Tonga submarine volcanic eruption. *The Seismic Record*, *2*(4), 217–226. https://doi.org/10.1785/0320220027

Turner, A. R. (2024). Shallow moonquake statistic. [ComputationalNotebook]. *Zenodo*. https://doi.org/10.5281/zenodo.13786113

Turner, A. R., Hawthorne, J. C., & Gaddes, M. (2022). Stresses in the lunar interior: Insights from slip directions in the A01 deep moonquake nest. *Journal of Geophysical Research: Planets*, *127*(12), e2022JE007364. https://doi.org/10.1029/2022JE007364

Vostreys, R. W. (1980). Data user's note: Apollo seismological investigations. *Technical Reports Series*.

Warren, N. W., & Latham, G. V. (1970). An experimental study of thermally induced microfracturing and its relation to volcanic seismicity. *Journal of Geophysical Research*, *75*(23), 4455–4464. https://doi.org/10.1029/jb075i023p04455

Watters, T. R., Johnson, C. L., & Schultz, R. A. (2010). Lunar tectonics. *Planetary tectonics*, *11*, 121–182. https://doi.org/10.1017/cbo9780511691645.005

Watters, T. R., Weber, R. C., Collins, G. C., Howley, I. J., Schmerr, N. C., & Johnson, C. L. (2019). Shallow seismic activity and young thrust faults on the moon. *Nature Geoscience*, *12*(6), 411–417. https://doi.org/10.1038/s41561-019-0362-2

Weber, R., Bills, B., & Johnson, C. (2009). Constraints on deep moonquake focal mechanisms through analyses of tidal stress. *Journal of Geophysical Research*, *114*(E5), E05001. https://doi.org/10.1029/2008je003286

Wiener, N. (1949). *Extrapolation, interpolation, and smoothing of stationary time series: With engineering applications*. The MIT Press.

Wyss, M., Shimazaki, K., & Wiemer, S. (1997). Mapping active magma chambers by b values beneath the off-Ito volcano, Japan. *Journal of Geophysical Research*, *102*(B9), 20413–20422. https://doi.org/10.1029/97jb01074